RSC Advances

ROYAL SOCIETY OF CHEMISTRY

www.rsc.org/advances

RSC Advances

RSCPublishing

PAPER

Stimuli-responsive protoporphyrin IX silica-based nanoparticles for photodynamic therapy *in vitro*

Cite this: DOI: 10.1039/x0xx00000x

Juan L. Vivero-Escoto*[a,b] and Daniel L. Vega[a,b]

Received 00th January 2012,
Accepted 00th January 2012

DOI: 10.1039/x0xx00000x

www.rsc.org/

Nanoparticle-based delivery systems have been explored recently as efficient vehicles to transport photosensitizers for photodynamic therapy (PDT). In this study; we report the synthesis, characterization and in *in vitro* application of a stimuli-responsive silica nanoparticle platform chemically functionalized with protoporphyrin IX (RR-PpIX-SiNPs). PpIX photosensitizers have been attached to the surface of SiNPs through a redox-responsive linker. PpIX molecules can be selectively released from RR-PpIX-SiNP platform in their monomeric form in the presence of the high reducing environment found in cancer cells. The structural, photophysical and photochemical properties of RR-PpIX-SiNPs were characterized and compared with a control sample (PpIX-SiNPs), which does not contained a redox-responsive linker. Cell viability measurements demonstrated that RR-PpIX-SiNPs were more phototoxic than PpIX-SiNPs. Confocal microscopy shows that RR-PpIX-SiNPs are mainly localized in lysosomes. Finally, the redox-responsive release of PpIX molecules was demonstrated in solution and in *in vitro* using UV-vis spectrometry and confocal microscopy, respectively. We envision that further modification of this platform can render colloidal stability and target-specific properties by grafting polymeric chains and small molecules or biomolecules.

1. Introduction

Photodynamic therapy (PDT) is an innovative minimally invasive therapy that has great potential to selectively destroy malignant cells while sparing the normal tissues. PDT is currently approved for the treatment of various types of cancers including lung, head and neck, esophageal and cervical.[1-4] Contrary to traditional cancer treatments, such as surgery, radiotherapy and chemotherapy, PDT can avoid undesirable side effects such as nausea and vomiting and, in some cases, suppression of the immune system, making it an ideal therapy for vulnerable patients. PDT is based on the photochemical reactions between a light-activated chemical (photosensitizer, PS) and light of an appropriate wavelength to afford cytotoxicity via the generation of reactive oxygen species (ROS).[5, 6] Upon successful activation via light energy transfer, the PS is promoted from its ground state (S_0) to the first excited singlet state (S_1) from which, through an intersystem crossing pathway, the energy is transferred to its longer-lived triplet state (T_1). Population of the triplet state is necessary in order to produce the ROS necessary to initiate cell death. In most cases, the key ROS of PDT is singlet oxygen ($^1O_2$).[4, 5] The PS is perhaps the most critical component of PDT and continues to be an area of intense scientific research.[7, 8] Traditionally, PS molecules based on porphyrins have dominated the field.[9, 10] For example, protoporphyrin IX (PpIX) is a naturally occurring porphyrin constituent of haemoglobin, Cytochrome *c* and other biologically relevant molecules. PpIX, a second generation PS, is produced in the body by the conversion of 5-aminolevulinic acid through the heme biosynthetic pathway.[2] Similar to other porphyrin-based PSs, PpIX has several disadvantages, such as low water solubility, cutaneous photosensitivity, and reduced selectivity for targeted tissues.[3, 11] Nanotechnology has emerged as an alternative approach to overcome some of the main delivery issues of PSs. Nanoparticles offer several advantages as PS delivery systems: they can carry a large payload of PS molecules; their surfaces and compositions can be tailored to develop multifunctional systems (e.g. target-specificity); and due to their small sizes, nanoparticles can penetrate deep into tissues and be readily internalized by cells.[12, 13] Several nanoparticulate platforms have been explored to deliver PS molecules such as liposomes, polymers, gold and iron oxide nanoparticles.[3, 12-14] Recently, silica-based nanoparticles (SiNPs) have attracted a great deal of attention as PS delivery systems due to their outstanding features of nontoxicity, tunable surface, chemical inertness and optical transparency.[12, 15] Prasad and Kopelman have been pioneers in this field. Kopelman and co-workers have published on the physical encapsulation of meta-tetra(hydroxyphenyl)chlorin or Foscan® and methylene blue inside silica nanoparticles.[16, 17] Prasad and co-workers reported on the encapsulation of 2-devinyl-2-(1-hexyloxyethyl)-pyropheophorbide (HPPH) and iodo-benzylpyro-silane by using organically modified silica (ORMOSIL) nanoparticles.[18, 19] ORMOSIL particles have also been used to incorporate other type of PS agents such as PpIX, Foscan® and silicon phthalocyanine Pc4.[20-23] Recently, mesoporous silica nanoparticles (MSNs) have attracted attention as carriers for PSs. Mou, Bein and others reported on the incorporation of PpIX, Pd-meso-tetra(4-carboxyphenyl) porphyrin, aluminium phthalocyanine-disulfonate, and zinc(II)

phthalocyanine with MSNs.[24-30] These papers reported PS loadings of 30-200 μmol per gram of nanoparticle. In all these approaches, the PS agents have been incorporated inside SiNPs by physical or chemical encapsulation. The first method is challenging due to the highly hydrophobic nature of the PS molecules, which result in aggregation and self-quenching inside of the SiNP carrier. Moreover, PSs usually leak from the silica matrix which can lead to a reduced efficiency of treatment and to side-effects. The second method can overcome some of these drawbacks, but aggregation and self-quenching of PS agents inside of nanoparticles may still occur.[15] Ideally, a PS delivery system for cancer treatment should avoid any leaking of PSs before reaching its target. However, once it is internalized by cancer cells, it should deliver the PS molecules in a selective fashion to avoid self-quenching due to aggregation.[13, 31] In this work, we report the synthesis, characterization and *in vitro* PDT application of redox-responsive PS-loaded silica nanoparticles. This platform contains solid SiNPs, whose surface has been modified with PpIX agents chemically attached through a redox-responsive linker (RR-PpIX-SiNPs). The ligand has a disulfide bond that can be broken under reducing conditions such as those found in cancer cells.[32, 33] We hypothesize that after internalization by cancer cells, the disulfide bond will be broken releasing the PpIX agents in monomeric form (Fig. 1). This approach will eliminate aggregation of the PpIX molecules, avoiding self-quenching and, as a consequence, increasing the PDT effect. RR-PpIX-SiNPs were synthesized by modifying the surface of SiNPs with a RR-PpIX silane ligand via a grafting method; in a similar way, a non-responsive silica material (PpIX-SiNPs) was synthesized using a control linker (PpIX-silane ligand) (Fig. S1†). The structural properties of RR- PpIX-SiNP and PpIX-SiNP materials, such as particle size, hydrodynamic diameter, surface charge and organic content were characterized. The photophysical and photochemical properties of both materials were also investigated. The biocompatibility and phototoxicity of RR-PpIX-SiNPs and PpIX-SiNPs were investigated by the MTS assay in human cervical cancer (HeLa) cells. In addition, the sub-cellular localization of these particles was investigated by confocal microscopy. Finally, the redox-responsive release of PpIX molecules was tested in solution under reducing conditions and further demonstrated *in vitro* by confocal microscopy.

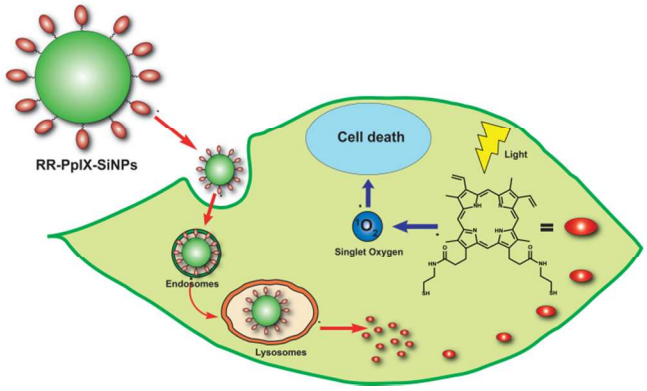

Fig.1 Schematic representation of the cellular internalization, redox-responsive release and phototoxic effect of RR-PpIX-SiNPs. Once the nanoparticles are internalized by cancer cells, the reducing environment affords the release of PpIX molecules in monomeric form and upon light exposure the photosensitizer generates singlet oxygen, which results in cell death.

2. Experimental details

2.1 Synthesis of protoporphyrin IX-silica nanoparticles (PpIX-SiNPs) and redox-responsive protoporphyrin IX-silica nanoparticles (RR-PpIX-SiNPs).

The synthesis of SiNPs was carried out by following the Stöber method.[34] In a scintillation vial; 5 mL of ethanol, 180 μL of water and 357 μL of ammonia were added and stirred for 5 min. To this solution, 200 μL of tetraethoxysilane (TEOS) were added dropwise and the final solution was stirred for 24 h at RT. To afford the fluorescein isothiocyanate (FITC) labeled SiNPs, 100 μL of a previously prepared FITC silane derivative solution was added to the procedure described above. By following this approach, the FITC dye derivative is chemically encapsulated inside the SiNPs. In this way, the silanols on the exterior surface of the nanoparticles are free for further functionalization. The FITC silane derivative solution was prepared according to the following method: FITC dye (1 mg) was reacted with aminopropyl triethoxysilane (AP-TES, 1 μL) in DMSO (300 μL) for 45 min at RT. To synthesize PpIX-SiNPs, the PpIX-APTES ligand was grafted onto the SiNPs (1:10 wt.) by stirring and refluxing (90 °C) the materials in ethanol for 8 h. The final material was centrifuged, the supernatant was collected and the particles were redispersed in fresh ethanol for additional washing. This protocol was repeated at least four times until minimum amount of ligand was detected by UV-Vis spectroscopy. Finally, the particles were stored in ethanol. The supernatant and washing solutions were then put together, the solvent was eliminated by a lyophilizer and the unreacted PpIX-APTES linker was stored for further quantification by UV-Vis as shown in the ESI†. A similar approach was used to synthesize RR-PpIX-SiNP particles, but grafting the PpIX-MPTES ligand. The synthesis and characterization of PpIX-APTES and PpIX-MPTES ligands are described in the ESI†.

2.2 Structural characterization of PpIX- and RR-PpIX-SiNPs.

Thermogravimetric analysis (TGA) was carried out with a Mettler Toledo TGA/SDTA851 instrument equipped with a platinum pan and using a heating rate of 5 °C/min under nitrogen. A Raith 150 Field Emission Scanning Electron Microscope (SEM) was used to determine particle size and morphology. Each SEM sample was prepared by suspending the nanoparticles in ethanol. A drop of the suspension was placed on a silicon wafer and the solvent was allowed to evaporate. Dynamic light scattering (DLS) and zeta potential measurements were carried out using a Malvern Instrument Zetasizer Nano.

2.3 Photophysical characterization of PpIX- and RR-PpIX-SiNPs.

A Cary 300 Bio UV/vis spectrometer and a Fluorolog spectrofluorometer were used to determine the absorption and fluorescence emission of the PpIX-SiNP and RR-PpIX-SiNP materials, respectively. The nanoparticles were redispersed in DMF with a concentration of 176.5 μg/mL. SiNPs and PpIX (2 μM) dissolved in DMF were used as control samples.

2.4 Measurement of singlet oxygen.

The generation of singlet oxygen by the PpIX-SiNPs and RR-PpIX-SiNPs was determined indirectly by using 1,3-

diphenylisobenzofuran (DBPF). The samples were immediately prepared before use by transferring 40 μL of DPBF stock solution (8 mM) to 4 mL of a suspension of PpIX-SiNPs or RR-PpIX-SiNPs in a quartz cuvette in the dark. The experiments were carried out by irradiating the samples with LumaCare LC122 light source (FOP LUM V 400-700 nm; 41 ± 2 mW/cm^2) for 10, 20 and 30 seconds. The decrease of DPBF absorbance at 415 nm was monitored with a Cary 300 Bio UV/vis spectrometer. SiNPs and PpIX molecules were used as control samples for this experiment.

2.5 Release profile of PpIX molecules from RR-PpIX-SiNPs under reducing conditions.

To determine the release of PpIX compound under simulated reducing conditions, the reducing agent dithiothreitol (DTT) was used. The RR-PpIX-SiNPs were redispersed in 10 mL of DMF with a concentration of 0.5 mg/mL. The dispersion was stirred for 20 h total under N_2 atmosphere to determine the amount of background PS agents. After that, the DMF was replaced with a 10 mL DMF solution of DTT (10 mM). Aliquots were taken at certain intervals of time and the absorption was measured to determine the amount of PpIX molecules released. A similar procedure was followed for PpIX-SiNP material, which was used as a control sample.

2.6 Cytotoxicity.

HeLa cells were seeded at a density of 1 x 10^4 cells/mL in a 96-well culture plates and incubated in 100 μL of RPMI-1640 cell media for 24 h at 37 °C with 5% CO_2. Cells were inoculated with varying dosages of SiNPs, PpIX-SiNPs and RR-PpIX-SiNPs (1, 10, 25, 50, 100, 150 and 200 μg/mL) for 48 h at 37 °C. The cells were washed twice with phosphate buffer solution (PBS) and 20 μL of Celltiter 96® was added to each well and incubated for another 3 h at 37 °C to evaluate the toxicity with the MTS assay. The absorbance was measured at a wavelength of 450 nm. Cell viability percentage was calculated based on the absorbance measured relative to that of control culture cells.

2.7 Phototoxicity.

HeLa cells were seeded at a density of 1 x 10^4 cells/mL in a 96-well cell plates and incubated in 100 μL of RPMI-1640 cell media for 24 h at 37 °C. Cells were then inoculated with SiNPs, PpIX-SiNPs and RR-PpIX-SiNPs (7, 14, 25, 50, 75 and 100 μg/mL) for 24 h in cell media, followed by PBS washing steps, and then further incubated in PBS for light exposure. Samples were exposed to a LumaCare LC122 light source (FOP LUM V 400-700 nm; 170 ± 3 mW/cm^2) for 20 min. After irradiation, the cells were incubated in cell media for 24 h and the cell survival was tested by the MTS assay. The absorbance was measured at a wavelength of 450 nm. Cell viability percentage was calculated based on the absorbance measured relative to that of control culture cells.

2.8 Internalization and subcellular localization of RR-PpIX-SiNP materials.

HeLa cells were seeded at a density of 5 x 10^4 cells/mL in a six-well culture plates with coverslips at the bottom of the wells and incubated in 3 mL of RPMI-1640 cell media for 24 h at 37 °C with 5% CO_2. The cell media was replaced by 3 mL of FITC-labeled RR-PpIX-SiNP materials (50 μg/mL) and incubated in the RPMI-1640 cell media. Endosomes, lysosomes and mitochondria were stained in independent experiments for confocal microscopy analysis. Endosomes were stained using the endosome marker FM® 4-64 dye (11.1 μg/mL) in the presence of FITC-labeled RR-PpIX-SiNPs for 6 h. To stain lysosomes, HeLa cells were incubated in the presence of RR-PpIX-SiNPs for 6 h, LysoTracker® Green DND-26 (5 μM) was added and the cells were incubated for additional 6 h. The mitochondria were labeled by incubating HeLa cells, previously inoculated with FITC-labeled RR-PpIX-SiNPs for 8 h, with MitoTracker® red CMXRos (200 nM) for 80 min. Finally, for each independent experiment, the cell-plated coverslips were washed twice with PBS buffer (1mM, pH 7.4) and stained with NucBlue® Live cell staining DAPI solution for 15 min. The stained coverslips were placed in microscope slides and examined under an Olympus Fluoview FV 1000 confocal fluorescence microscope system.

2.9 Phototoxic effect and i*n vitro* redox-responsive release of PpIX molecules from FITC-labeled RR-PpIX-SiNPs.

The phototoxic effect and release *in vitro* of PpIX molecules from FITC-labeled RR-PpIX-SiNPs was investigated by confocal microscopy. HeLa cells were seeded at a density of 5 x 10^4 cells/mL in a six-well culture plates with coverslips at the bottom of the wells and incubated in 3 mL of RPMI-1640 cell media for 24 h at 37 °C with 5% CO_2. The cell media was replaced by 3 mL of FITC-labeled RR-PpIX-SiNP materials (50 μg/mL) and incubated in the RPMI-1640 cell media for 12 h. Cell plates were exposed to LumaCare LC122 light source (FOP LUM V 400-700 nm; 170 ± 3 mW/cm^2) for 20 min. After irradiation, the cells were incubated in cell media for another 24 h. Finally, the cell-plated coverslips were washed twice with PBS buffer (1mM, pH 7.4) and stained with NucBlue® Live cell staining solution for 15 min. The stained coverslips were placed in microscope slides and examined under an Olympus Fluoview FV 1000 confocal fluorescence microscope system.

3. Results and discussion

3.1 Preparation and characterization of PpIX-SiNPs and RR-PpIX-SiNPs

3.1.1. Synthesis of PpIX-SiNPs and RR-PpIX-SiNPs. To construct the PpIX-SiNP and RR-PpIX-SiNP carrier systems, we first synthesized the silyl functionalized PpIX-APTES and PpIX-MPTES ligands. The experimental details for the synthesis and characterization of these ligands are described in the ESI† and Fig. S1†. Solid SiNPs, which were previously synthesized following the Stöber method, were functionalized with PpIX-APTES and PpIX-MPTES ligands by grafting these silane derivatives onto the surface of the SiNPs in refluxing ethanol. The resulting PpIX-SiNP and RR-PpIX-SiNP materials were isolated and purified as described in the experimental section.

3.1.2. Characterization of PpIX-SiNPs and RR-PpIX-SiNPs. The structural properties of PpIX-SiNP and RR-PpIX-SiNP carriers were characterized by scanning electron microscopy (SEM) and dynamic light scattering (DLS). The micrographs of both PpIX-SiNP and RR-PpIX-SiNP materials show monodisperse spherical particles with an average particle diameter of 300 nm (Fig. 2 and Table 1). DLS measurements of naked SiNPs in ethanol confirm the size of the nanoparticles; however, after grafting of the PpIX-silane derivatives, the hydrodynamic diameter in both ethanol and water increased considerably due to aggregation of the hydrophobic PpIX-SiNP and RR-PpIX-

SiNP particles. The surface properties of these materials were characterized by ζ–potential and thermogravimetric analysis (TGA). The ζ–potential measurements of both functionalized nanoparticles show neutral surface charge as an indication of the successful functionalization of these materials (Table 1). Moreover, TGA shows a loading of the PpIX-silane ligands of 116.7 and 85.7 μmol of PS per gram of material for PpIX-SiNPs and RR-PpIX-SiNPs, respectively. This loading was further confirmed by UV-vis spectroscopy obtaining a loading of the PpIX-silane ligands of 98.5 and 82.8 μmol of PS per gram of material for PpIX-SiNPs and RR-PpIX-SiNPs, respectively. These PS loadings are in the range to what has been reported previously in the literature.

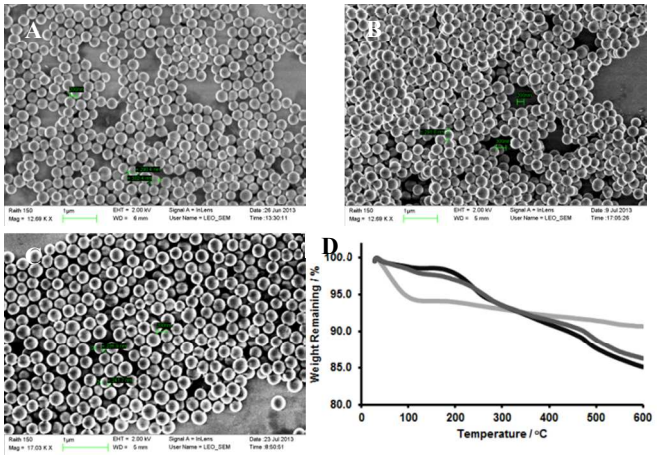

Fig. 2 SEM images of A) SiNPs, B) PpIX-SiNPs and C) RR-PpIX-SiNPs. D) Organic content of SiNPs (light gray), PpIX-SiNPs (gray) and RR-PpIX-SiNPs (black) determined by TGA.

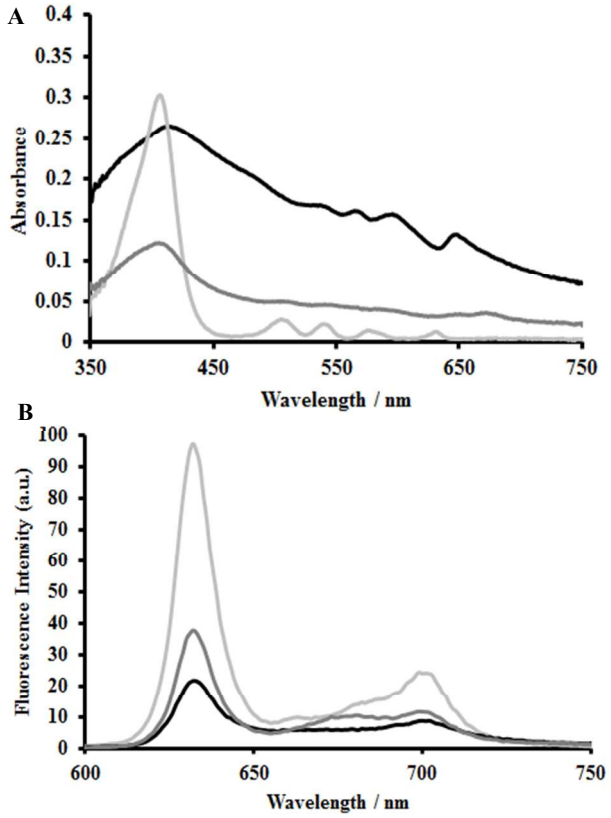

Fig. 3 A) Absorption and B) emission spectra of PpIX (light gray), PpIX-SiNPs (gray) and RR-PpIX-SiNPs (black) in DMF solution.

Table 1. Structural properties of PpIX-SiNPs and RR-PpIX-SiNPs. The DLS was measured in ethanol and water (data in parenthesis).

Sample	DLS (nm)	PDI	(SEM) (nm)	ξ-potential (mV)	Amount of ligand (μmol/g)
SiNPs	338 (350)	0.15 (0.35)	298±30	-11.0±0.9	---
PpIX-SiNPs	1074 (1690)	0.24 (0.75)	310±25	-6.5±0.5	116.7
RR-PpIX-SiNPs	1042 (1850)	0.19 (0.64)	309±20	-5.3±0.5	85.7

3.1.3. Photophysical and photochemical characterization of PpIX-SiNPs and RR-PpIX-SiNPs. The photophysical properties of PpIX-SiNP and RR-PpIX-SiNP particles were investigated by UV-vis and fluorescence spectroscopy, while $^1O_2$ generation was used to measure their photochemical properties. The absorption and emission spectra of PpIX-SiNP and RR-PpIX-SiNP particles in DMF suspension, of the PpIX-silane ligands, and of free PpIX are shown in Fig. 3A and 3B, respectively. The absorption maxima correspond to the Soret band (ca. 410 nm) and the Q bands (500-650 nm) were detected in the PpIX molecules. These bands were also observed in the suspension of both PpIX-SiNP and RR-PpIX-SiNP materials, although the bands are overlapped and red-shifted related to PpIX by the light scattering of the solid particles, which is responsible for spectral broadening.[35] The emission bands of PpIX-SiNP and RR-PpIX-SiNP particles in DMF solution (λ_{em} = 632 nm and 699 nm) were similar to the emission spectrum of PpIX molecules in the same solution (0.1 μM) (Fig. 3B). The generation of $^1O_2$ in DMF solution was estimated indirectly using DPBF as a singlet oxygen chemical probe. DPBF reacts irreversibly with $^1O_2$ and the reaction can be easily followed with spectrophotometry by recording the decrease in the intensity of the DPBF absorption at around 415 nm.[36] The changes in DPBF oxidation with time upon light exposure (400-700 nm; 41 ± 2 mW/cm^2) in the presence of PpIX-SiNPs and RR-PpIX-SiNPs can be seen in Fig. S3†. Moreover, the experiment also depicts the lack of DPBF oxidation in the presence of SiNPs after light exposure, which demonstrates that the oxidation of DPBF is induced by singlet oxygen. Control experiments showed the photophysical stability of DPBF and PpIX under our experimental conditions (data not shown). Light exposure of PpIX-SiNP and RR-PpIX-SiNP materials during 10, 20 and 30 seconds causes lower DPBF oxidation compared with PpIX molecules upon similar conditions. This difference in $^1O_2$ generation between PS encapsulated nanoparticles and the parent PS molecule has been previously reported in the literature.[17, 37] In those reports, it was assumed that scattering of the nanoparticles and local sequestration of $^1O_2$ could be the reasons for the lower $^1O_2$ production. However, in our case, we hypothesize that the aggregation of the PpIX-functionalized SiNPs due to their hydrophobic surfaces is the main reason for the difference in $^1O_2$ generation. It is known that aggregation reduces the quantum yield and the lifetime of the excited triplet state of porphyrins and, consequently, should reduce $^1O_2$ generation.[13]

3.1.4. Release profile of PpIX molecules under reducing conditions from PpIX-SiNP and RR-PpIX-SiNP materials. The RR-PpIX-SiNP particles were designed to be stable under normal physiological conditions, but readily degrade to release the PpIX molecules upon the reductive cleavage of the disulfide bonds by endogenous biomolecules, such as glutathione and cysteine. Release experiments revealed that both PpIX-SiNP and RR-PpIX-SiNP particles are stable in the absence of reducing agents, with only 5% or less background release over a few hours (Fig. 4). However, after the addition of 10 mM dithiothreitol (DTT), PpIX molecules were quickly released from the RR-PpIX-SiNPs with a half-life ($t_{1/2}$) of 10 h. In these particles, more than 90% of the PpIX molecules were released after six days of incubation with DTT. By contrast, the PpIX-SiNPs, our control materials, show less than 25% release after 10 days of incubation.

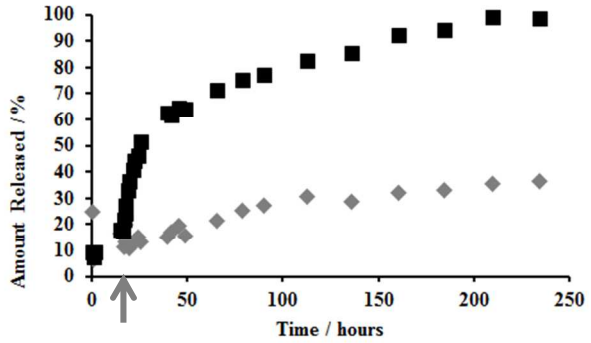

Fig. 4 Release profile of PpIX molecules under reducing conditions from PpIX-SiNPs (gray) and RR-PpIX-SiNPs (black). The gray arrow indicates the time at which the reducing agent DTT was added.

3.2 Cyto and phototoxicity of PpIX-SiNPs and RR-PpIX-SiNPs

The biocompatibility of PpIX-SiNP and RR-PpIX-SiNP materials in the absence of light was tested in HeLa cells using the MTS assay. The cell survival data demonstrated that PpIX-SiNP and RR-PpIX-SiNP materials are fairly biocompatible in concentrations as high as 150 μg/mL (Fig. 5). Moreover, their biocompatibility is similar to non-functionalized SiNPs, which indicates that grafting the PpIX ligands outside the nanoparticle does not increase the toxicity of the materials in the absence of light. The phototoxicity of PpIX-SiNPs and RR-PpIX-SiNPs, at different concentrations of materials, was tested under light exposure (400-700 nm; 170 ± 3 mW/cm^2) for 20 min. Fig. 6 shows the cell survival of HeLa cells that have been incubated

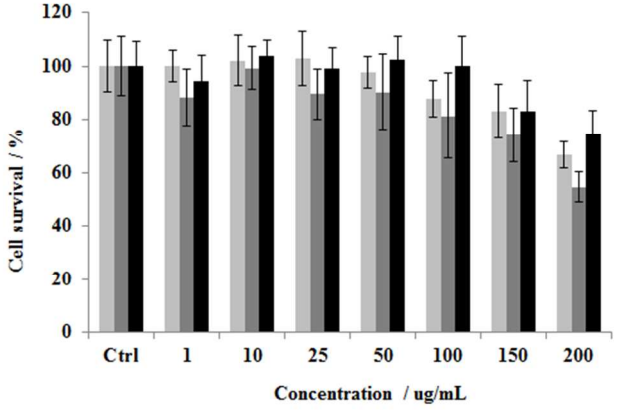

Fig. 5 Biocompatibility of SiNPs (light gray), PpIX-SiNPs (gray) and RR-PpIX-SiNPs (black) measured by MTS assay.

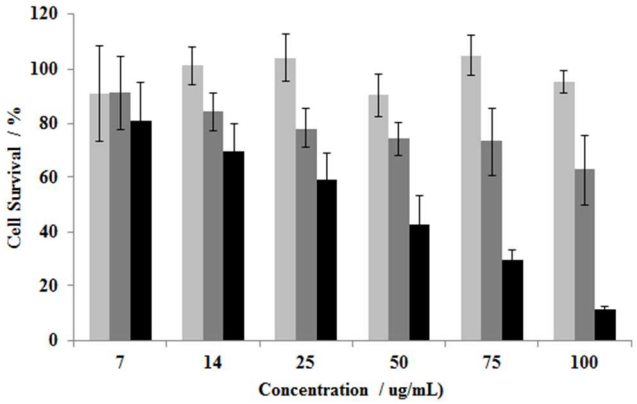

Fig. 6 Cytotoxicity of SiNPs (light gray), PpIX-SiNPs (gray) and RR-PpIX-SiNPs (black), after light exposure (400-700 nm; 170 ± 3 mW/cm^2) for 20 min, measured by MTS assay.

for 24 h after light irradiation. SiNPs did not show a significant phototoxic effect. However, the cell viability decreased in the presence of PpIX-SiNP and RR-PpIX-SiNP particles after light exposure. Noteworthy, the decrease in cell survival is more dramatic with RR-PpIX-SiNPs as an indication of the capability of this material to deliver PpIX molecules in monomeric form under intracellular reducing conditions and without loss of photoactivity. The IC_{50} for this material is between 25-50 μg/mL, which is roughly equivalent to 2.15 – 4.3 μM of PS agent based on TGA data. However, the IC_{50} for PpIX-SiNPs is above 100 μg/mL (11.7 μM). This shows that redox-responsive silica-based materials can deliver the PS agents as individual units, thereby avoiding aggregation and self-quenching, which improve the PDT effect. Nevertheless, the PDT efficacy of this material is still lower than PpIX in solution (IC_{50} ~ 1 μM) (Fig. S4†). We hypothesize that the hydrophobicity of the nanoparticles is affecting both their cellular internalization and release of PpIX molecules, which results in the reduction of the PDT effect. Control experiments of SiNPs, PpIX-SiNPs and RR-PpIX-SiNPs under similar conditions, but in the absence of light did not show any considerable cytotoxic effect (Fig. S5†).

3.3 Internalization, subcellular localization and *in vitro* PpIX delivery from RR-PpIX-SiNPs

3.3.1. Intracellular uptake and subcellular localization of PpIX-SiNPs and RR-PpIX-SiNPs. Confocal microscopy was used to examine the internalization of PpIX-SiNP and RR-PpIX-SiNP materials in HeLa cells. The micrographs show that both PpIX-SiNPs and RR-PpIX-SiNPs are readily internalized by HeLa cells (Fig. 7B-C). To investigate the subcellular location of RR-PpIX-SiNPs the material was labeled with FITC

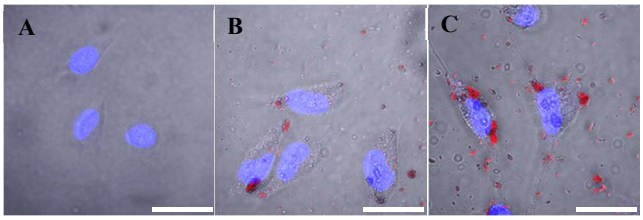

Fig. 7 Confocal fluorescence images of HeLa cells. A) Control sample without nanoparticles, B) PpIX-SiNPs and C) RR-PpIX-SiNPs. The images show the overlapping of DAPI-stained nuclei (blue), red fluorescence of PpIX-grafted particles and cell body (DIC channel). Scale bar = 20 μm.

dye by chemically encapsulating the dye molecule inside of the nanoparticles. Endosomes were tagged with endosome marker FM® 4-64 dye and incubated in the presence of FITC-labeled RR-PpIX-SiNPs for 6 h. Fig. 8A-C show that under those experimental conditions, FITC-labeled RR-PpIX-SiNPs are not co-localized with endosomes. Lysosomes were labeled with LysoTracker® Green DND-26 and incubated in the presence of RR-PpIX-SiNPs for 12 h total. The micrographs (Fig. 8D-F) show the co-localization of RR-PpIX-SiNP material and lysosomes (white arrows). In this experiment, the RR-PpIX-SiNPs were not labeled with FITC, moreover, the particles were imaged using the DIC channel. These data might indicate the RR-PpIX-SiNPs are transported by an endolysosomal pathway, which is a common route of internalization for SiNPs.[38] Nevertheless, additional experiments are necessary to investigate the endocytic mechanism and the dynamics of intracellular transporting, which are out of the scope of this work. Previous reports have shown that PS-loaded SiNPs (30 nm in diameter) can be localized inside the mitochondria.[23] To test that possibility with RR-PpIX-SiNPs; HeLa cells, previously inoculated with FITC-labeled RR-PpIX-SiNPs, were tagged with MitoTracker® red CMXRos dye. Confocal images show that RR-PpIX-SiNPs are not co-localized with MitoTracker® dye (Fig. 8G-I); presumably due the size of these nanoparticles.

3.3.2. *In vitro* PpIX delivery from RR-PpIX-SiNPs. To investigate the intracellular redox-responsive release of PpIX molecules from RR-PpIX-SiNPs, confocal micrographs of the FITC-labeled material after exposure with light and incubation for 24 h were taken (Fig. 9). To perform this experiment, we

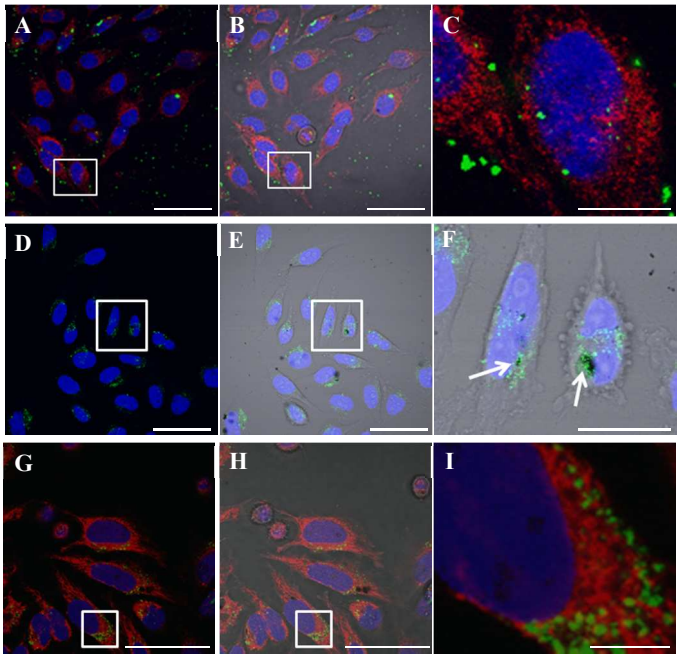

Fig. 8 Confocal fluorescence images of HeLa cells loaded with RR-PpIX-SiNPs (green). A-C) Endosomes were labeled with FM® 4-64 dye (red). D-F) Lysosomes were tagged with LysoTracker® Green DND-26 (green) and the RR-PpIX-SiNPs were imaged using the DIC channel. G-I) Mitochondria was labeled using MitoTracker® red CMXRos dye (red). Scale bars = 25 μm (A,B,D,E, G and H); 10 μm (C); 15 μm (F); 5 μm (I).

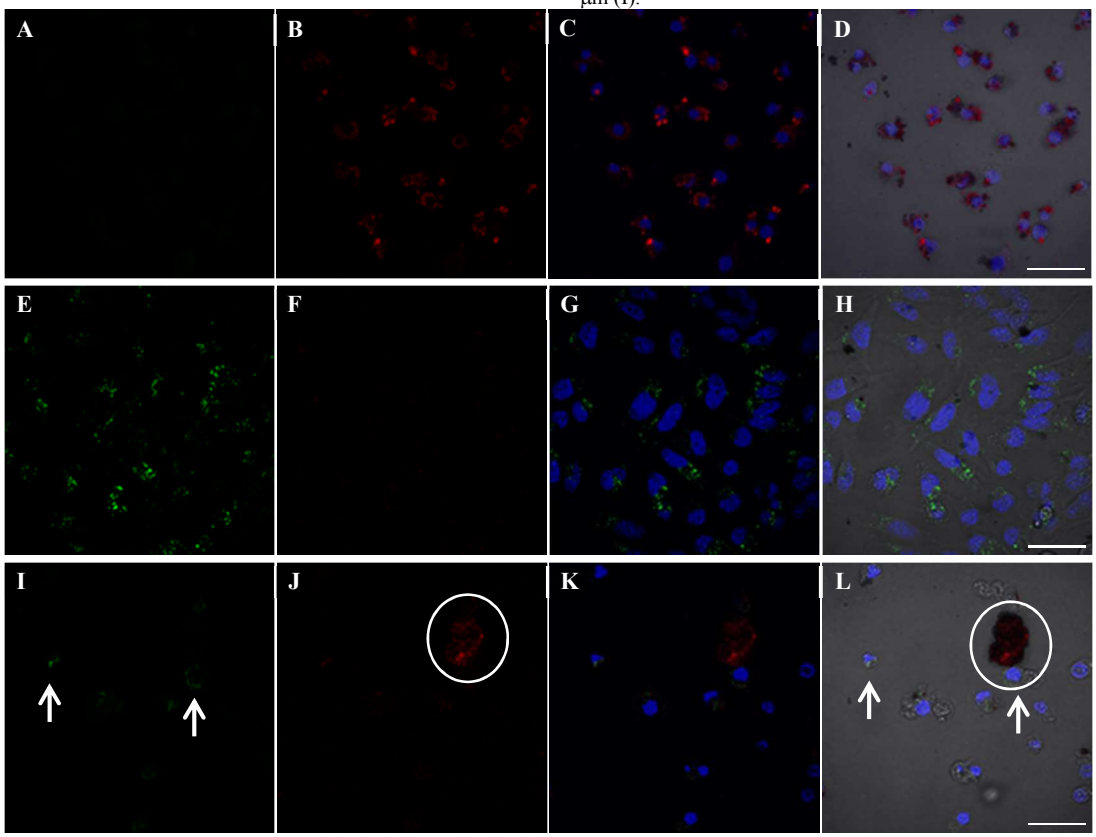

Fig. 9 Confocal fluorescence images of HeLa cells inoculated with PpIX in solution (A-D), PpIX-SiNPs (E-H), and RR-PpIX-SiNPs (I-L). Green fluorescence of the FITC-functionalized nanoparticles (A,E,I); red fluorescence of PpIX molecules (B,F, J); the overlapped imaged of green, red and DAPI-stained nuclei (C,G,K); and the overlapped imaged with the DIC channel (D,H,L). Scale bars = 30 μm (A-D & I-L); 20 μm (E-H). The circles show the release of PpIX molecules and the arrows show the presence of the FITC-labeled RR-PpIX-SiNPs.

took advantage of examining the FITC-labeled RR-PpIX-SiNPs (green channel) and PpIX molecules (red channel) using different channels in confocal microscopy. In principle, once the PpIX molecules have been released from the FITC-labeled RR-PpIX-SiNPs, we will be able to visualize the green and red fluorescence of the SiNPs and the released PpIX molecules in the same confocal micrograph (Fig. 9I-L). To corroborate our observations, control experiments using PpIX in solution and FITC-labeled PpIX-SiNPs under the same experimental conditions were also carried out. Interestingly, confocal micrographs (Fig. 9A-D) show a major phototoxic effect on HeLa cells in the presence of PpIX solution (1 μM). In addition, PpIX molecules appear to be accumulated in some kind of black material, which is presumably debris of cells death. By contrast, the confocal images for FITC-labeled PpIX-SiNP particles did show neither phototoxicity nor any release of PpIX molecules (Fig. 9E-H). In the case of the FITC-labeled RR-PpIX-SiNPs, the confocal micrographs clearly show the PDT effect and the presence of both FITC-labeled SiNPs (green fluorescence) and PpIX molecules (red fluorescence) as an indication of the successful release of PpIX molecules from RR-PpIX-SiNPs (Fig. 9I-L). Additional confocal images are shown in the ESI† (Fig. S6†); which further support this observation. These data demonstrate that the redox-responsive platform indeed released the PpIX molecules inside HeLa cells producing a higher PDT effect compared with the control experiment (PpIX-SiNPs).

4. Conclusions

We have designed, synthesized and characterized a silica-based platform to carry and release photosensitizers under intracellular reducing environment and with improved phototoxic effect. The RR-PpIX-SiNPs are 300 nm in diameter according to scanning electron microscopy. Dynamic light scattering and ζ–potential show that the surface of the particles is hydrophobic due to the presence of PpIX molecules. This hydrophobicity also impacts negatively the generation of $^1O_2$ because of aggregation and self-quenching. The redox-responsive properties of the RR-PpIX-SiNP platform were tested in solution using DTT as reducing agent. Confocal micrographs further demonstrated the successful release of PpIX molecules *in vitro*. The RR-PpIX-SiNPs are readily internalized by HeLa cells as shown by confocal images; in addition, they are biocompatible in the absence of light as was determined by MTS assay. The PDT efficacy of RR-PpIX-SiNPs was evaluated under light exposure for 20 min using the MTS assay after 24 h of incubation. The redox-responsive system showed a higher phototoxicity than the control sample. Presumably, because of the intracellular release of PpIX molecules avoids the aggregation and self-quenching of PS agents. RR-PpIX-SiNPs are internalized by HeLa cells and are transported by endolysosomal pathway according to our preliminary subcellular localization experiments. Overall, our data prove that by developing redox-responsive silica nanoparticles that selectively release PS agents inside the cells, the PDT efficacy can be enhanced. This platform needs further improvement to expand its scope toward *in vivo* application. Nanoparticles can be functionalized with polymers such as poly(ethylene glycol) and targeting agents to improve their colloidal properties and targeting ability. Our group is currently working on the design of the building blocks to achieve these goals.

Acknowledgements

The authors would like to thank UNC-Charlotte (start-up, FRG program and CLAS seed money) and the Nanoscale Science program for financial support. The Department of Biology at UNC-Charlotte for allowing us to use their confocal microscopy facilities. Dr. Richard Jew for critical reading of the manuscript and helpful suggestions.

Notes and references

[a] Department of Chemistry, University of North Carolina at Charlotte, Charlotte, NC 28223, USA. E-mail: jviveroe@uncc.edu

[b] The Center for Biomedical Engineering and Science, University of North Carolina at Charlotte, Charlotte, NC 28223, USA.

† Electronic Supplementary Information (ESI) available: synthesis and characterization of PpIX-APTES and PpIX-MPTES; quantification of PpIX-APTES and PpIX-MPTES ligands; singlet oxygen generation; photo- and cytotoxicity of PpIX in solution; cytotoxicity of SiNPs, PpIX-SiNPs and RR-PpIX-SiNPs; and *in vitro* release of PpIX molecules. See DOI: 10.1039/b000000x/

1 J. P. Celli, B. Q. Spring, I. Rizvi, C. L. Evans, K. S. Samkoe, S. Verma, B. W. Pogue, T. Hasan, *Chem. Rev.* 2010, **110**, 2795-2838.

2 A. E. O'Connor, W. M. Gallagher, A. T. Byrne, *Photochem. Photobiol.* 2009, **85**, 1053-1074.

3 K. Chatterjee Dev, S. Fong Li, Y. Zhang, *Adv Drug Deliv Rev* 2008, **60**, 1627-37.

4 W. M. Sharman, C. M. Allen, J. E. van Lier, *Drug Discovery Today* 1999, **4**, 507-517.

5 S. Yano, S. Hirohara, M. Obata, Y. Hagiya, S.-i. Ogura, A. Ikeda, H. Kataoka, M. Tanaka, T. Joh, *J. Photochem. Photobiol., C* 2011, **12**, 46-67.

6 A. Juarranz, P. Jaen, F. Sanz-Rodriguez, J. Cuevas, S. Gonzalez, *Clin. Transl. Oncol.* 2008, **10**, 148-154.

7 R. R. Allison, C. H. Sibata, *Photodiagn. Photodyn. Ther.* 2010, **7**, 61-75.

8 M. R. Detty, S. L. Gibson, S. J. Wagner, *J. Med. Chem.* 2004, **47**, 3897-3915.

9 M. Ethirajan, Y. Chen, P. Joshi, R. K. Pandey, *Chem. Soc. Rev.* 2011, **40**, 340-362.

10 L. B. Josefsen, R. W. Boyle, *Theranostics* 2012, **2**, 916-966.

11 R. R. Allison, H. C. Mota, V. S. Bagnato, C. H. Sibata, *Photodiagnosis Photodyn Ther* 2008, **5**, 19-28.

12 R. Chouikrat, A. Seve, R. Vanderesse, H. Benachour, M. Barberi-Heyob, S. Richeter, L. Raehm, J. O. Durand, M. Verelst, C. Frochot, *Curr. Med. Chem.* 2012, **19**, 781-792.

13 A. Master, M. Livingston, A. Sen Gupta, *J. Controlled Release* 2013, **168**, 88-102.

14 E. Paszko, C. Ehrhardt, M. O. Senge, D. P. Kelleher, J. V. Reynolds, *Photodiagn. Photodyn. Ther.* 2011, **8**, 14-29.

15 P. Couleaud, V. Morosini, C. Frochot, S. Richeter, L. Raehm, J.-O. Durand, *Nanoscale* 2010, **2**, 1083-1095.

16 F. Yan, R. Kopelman, *Photochem. Photobiol.* 2003, **78**, 587-591.

17 W. Tang, H. Xu, R. Kopelman, M. A. Philbert, *Photochem. Photobiol.* 2005, **81**, 242-249.

18 I. Roy, T. Y. Ohulchanskyy, H. E. Pudavar, E. J. Bergey, A. R. Oseroff, J. Morgan, T. J. Dougherty, P. N. Prasad, *J. Am. Chem. Soc.* 2003, **125**, 7860-7865.

19 T. Y. Ohulchanskyy, I. Roy, L. N. Goswami, Y. Chen, E. J. Bergey, R. K. Pandey, A. R. Oseroff, P. N. Prasad, *Nano Lett.* 2007, **7**, 2835-2842.
20 V. Simon, C. Devaux, A. Darmon, T. Donnet, E. Thienot, M. Germain, J. Honnorat, A. Duval, A. Pottier, E. Borghi, L. Levy, J. Marill, *Photochem. Photobiol.* 2010, **86**, 213-222.
21 J. Qian, A. Gharibi, S. He, *J. Biomed. Opt.* 2009, **14**, 014012-014016.
22 C. Compagnin, L. Bau, M. Mognato, L. Celotti, G. Miotto, M. Arduini, F. Moret, C. Fede, F. Selvestrel, I. M. Rio Echevarria, F. Mancin, E. Reddi, *Nanotechnology* 2009, **20**, 345101-345112.
23 B. Zhao, J.-J. Yin, P. J. Bilski, C. F. Chignell, J. E. Roberts, Y.-Y. He, *Toxicol. Appl. Pharmacol.* 2009, **241**, 163-172.
24 H.-L. Tu, Y.-S. Lin, H.-Y. Lin, Y. Hung, L.-W. Lo, Y.-F. Chen, C.-Y. Mou, *Adv. Mater.* 2009, **21**, 172-177.
25 M. P. Dobay, A. Schmidt, E. Mendoza, T. Bein, J. O. Raedler, *Nano Lett.* 2013, **13**, 1047-1052.
26 I. T. Teng, Y.-J. Chang, L.-S. Wang, H.-Y. Lu, L.-C. Wu, C.-M. Yang, C.-C. Chiu, C.-H. Yang, S.-L. Hsu, J.-a. A. Ho, *Biomaterials* 2013, **34**, 7462-7470.
27 S.-H. Cheng, C.-H. Lee, C.-S. Yang, F.-G. Tseng, C.-Y. Mou, L.-W. Lo, *J. Mater. Chem.* 2009, **19**, 1252-1257.
28 S. A. Mackowiak, A. Schmidt, V. Weiss, C. Argyo, C. von Schirnding, T. Bein, C. Braeuchle, *Nano Lett.* 2013, **13**, 2576-2583.
29 J. Tu, T. Wang, W. Shi, G. Wu, X. Tian, Y. Wang, D. Ge, L. Ren, *Biomaterials* 2012, **33**, 7903-7914.
30 D. Brevet, M. Gary-Bobo, L. Raehm, S. Richeter, O. Hocine, K. Amro, B. Loock, P. Couleaud, C. Frochot, A. Morere, P. Maillard, M. Garcia, J.-O. Durand, *Chem. Commun.* 2009, 1475-1477.
31 B. Chen, W. Pogue Brian, T. Hasan, *Expert Opin Drug Deliv* 2005, **2**, 477-87.
32 R. Mortera, J. Vivero-Escoto, I. I. Slowing, E. Garrone, B. Onida, V. S. Y. Lin, *Chem. Commun.* 2009, 3219-3221.
33 J. L. Vivero-Escoto, K. M. L. Taylor-Pashow, R. C. Huxford, J. Della Rocca, C. Okoruwa, H. An, W. Lin, W. Lin, *Small* 2011, **7**, 3519-3528.
34 W. Stoeber, A. Fink, E. Bohn, *J. Colloid Interface Sci.* 1968, **26**, 62-69.
35 L. M. Rossi, P. R. Silva, L. L. R. Vono, A. U. Fernandes, D. B. Tada, M. S. Baptista, *Langmuir* 2008, **24**, 12534-12538.
36 A. Gomes, E. Fernandes, J. L. F. C. Lima, *J. Biochem. Biophys. Methods* 2005, **65**, 45-80.
37 D. B. Tada, L. L. R. Vono, E. L. Duarte, R. Itri, P. K. Kiyohara, M. S. Baptista, L. M. Rossi, *Langmuir* 2007, **23**, 8194-8199.
38 J. L. Vivero-Escoto, I. I. Slowing, B. G. Trewyn, V. S. Y. Lin, *Small* 2010, **6**, 1952-1967.

